Helmholtz-Zentrum Geesthacht
Zentrum für Material- und Küstenforschung

Final Draft
of the original manuscript:

Razzaq, M.Y.; Behl, M.; Lendlein, A.:
Thermally-Induced Actuation of Magnetic Nanocomposites Based on Oligo(Omega-Pentadecalactone) and Covalently Integrated Magnetic Nanoparticles
In: MRS Advances (2018) Cambridge University Press

DOI: 10.1557/adv.2018.613

THERMALLY-INDUCED ACTUATION OF MAGNETIC NANOCOMPOSITES BASED ON OLIGO(*ω*-PENTADECALACTONE) AND COVALENTLY INTEGRATED MAGNETIC NANOPARTICLES

M. Yasar Razzaq,[a] M. Behl,[a] A. Lendlein[a,b]

[a]*Institute of Biomaterial Science, Helmholtz-Zentrum Geesthacht, Kantstr. 55, 14513 Teltow, Germany*
[b]*Institute of Chemistry, University of Potsdam, Karl-Liebknecht-Str. 24-25, 14476 Potsdam, Germany*

Abstract

The incorporation of inorganic particles in a polymer matrix has been established as a method to adjust the mechanical performance of composite materials. We report on the influence of covalent integration of magnetic nanoparticles (MNP) on the actuation behavior and mechanical performance of hybrid nanocomposite (H-NC) based shape-memory polymer actuators (SMPA). The H-NC were synthesized by reacting two types of oligo(*ω*-pentadecalactone) (OPDL) based precursors with terminal hydroxy groups, a three arm OPDL (^{3}AOPDL, M_n = 6000 g mol·1^{-1}) and an OPDL (M_n =3300 g · mol^{-1}) coated magnetite nanoparticle ($Ø$ = 10 ± 2 nm), with a diisocyanate. These H-NC were compared to the homopolymer network regarding the actuation performance, contractual stress (σ_{contr}) as well as thermal and mechanical properties. The melting range of the OPDL crystals ($\Delta T_{m,OPDL}$) was shifted in homo polymer networks from 36 °C – 76 °C to 41°C – 81 °C for H-NC with 9 wt% of MNP content. The actuators were explored by variation of separating temperature (T_{sep}), which splits the OPDL crystalline domain into actuating and geometry determining segments. T_{sep} was varied in the melting range of the nanocomposites and the actuation capability and contractual stress (σ_{contr}) of the nanocomposite actuators could be adjusted. The reversible strain (ε_{rev}) was decreased from 11 ± 0.3% for homo polymer network to 3.2±0.3% for H-NC9 with 9 wt% of MNP indicating a restraining effect of the MNP on chain mobility. The results show that the performance of H-NCs in terms of thermal and elastic properties can be tailored by MNP content, however for higher reversible actuation, lower MNP contents are preferable.

Introduction

Polymeric actuators are key components for many fold technical applications ranging from soft robots to medical devices and morphing structures [1-3]. Various polymeric actuators based on hydrogels [4-7], liquid-crystalline elastomers [8-10] or

electroactive polymers [11-14] have been realized. Among these materials, shape-memory polymer actuators (SMPA) offer an advantage of reprogrammable shapes with an erasable memory and have become a valuable option for versatile applications [15-17]. Thermally triggered SMPA base on crystallizable polymer networks with phase-segregated morphology of actuating (AD) and geometry determining (GDs) domains. Here, a conformational orientation of the ADs during programming resulted in reversible shape change of the sample during crystallization and melting process [15]. Nevertheless, polymeric actuators generally have low Young's moduli and because if this, low values of contractual stress (σ_{contr}) during actuation.

The mechanical performance of polymeric materials in terms of elastic modulus and strength can be improved by incorporation of nanoparticles (NPs) [18, 19]. A significant challenge for this approach is the control over the dispersion of the NPs in the polymer matrices and the particle-polymer interfacial interaction [20]. We hypothesized that the incorporation of magnetic nanoparticles (MNP) as filler will influence the elastic modulus and the σ_{contr} of the SMPA. However, the physical mixing of the MNP results in agglomeration and non-homogenous distribution because of the unfavorable entropic interaction between the polymer matrix and the MNPs. Such mixing procedures exert deleterious effects on the mechanical properties of the nanocomposites [20-22].

Our concept to address the sedimentation and agglomeration is the covalent integration of the MNP into the polymer matrix resulting in hybrid nanocomposites (H-NC). These H-NCs provide a uniform distribution of NPs with minimum effect on the crystallinity of the polymer network and were capable of magnetically controlled reversible actuation when a constant stress was applied [23]. However, the constant stress cannot be applied conveniently for certain applications. Recently, a magnetically controlled stress-free actuation was observed in a multiphase nanocomposite with two phase segregated crystallizable units, along with covalently integrated magnetic nanoparticles (MNP). Here, the crystallizable domain with higher melting point ($T_{m,GU}$) acted a geometry stabilizing unit (GU), while the domain with lower ($T_{m,\,AU}$) acted as actuation unit (AU) [24]. A magneto-mechanical deformation process ($> T_{m,GU}$) established the desired programmed shape and the MIC and CIE of the oriented AU by AMF (on-off) enabled reversible actuation. However, the heterogeneous morphology of these nancomposites significantly affected the distribution of the MNP in the polymer matrix.

Our strategy to realize a homogeneous morphology in H-NC bases on crystallizable oligomers using the same type of repeating unit. The synthesis of H-NCs was carried out by in situ condensation of an oligo(ω-pentadecalactone) (OPDL)-macrotriol (^{3}AOPDL), and OPDL coated iron(III)oxide MNP (OPDL@MNP) with 1,6-hexane diisocyanate (HDI) as reported in [23]. An ^{3}AOPDL with M_n = 6000 g·mol^{-1}and an OPDL@MNP that has surface grafted OPDL with M_n = 3300 g·mol^{-1}, were selected to enable the same melting point (T_m) of both precursors [25]. Variation of the ^{3}AOPDL to OPDL@MNP ratio in the reaction mixture resulted in H-NCs with 5 to 9 wt% of MNP. The nanocomposites were named as H-NCX, where X is the wt% of MNP, while the homo OPDL network synthesized without the addition of OPDL@MNP was named as N-OPDL. Along with thermal and mechanical analysis, specific thermomechanical experiments were designed to explore the effects of different content of MNP on the actuation capability under stress-free conditions and σ_{contr} generated during strain-controlled experiments.

Experimental details

The synthesis of OPDL based precursors ^{3}AOPDL and OPDL@MNP was carried out according to the reported procedures [23, 25]. In the following the synthesis of H-NC is exemplarily described for H-NC9: 0.7 g (0.015 mmol of hydroxyl groups) of

OPDL@MNP and 2.3 g (0.4 mmol) of ^{3}AOPDL were reacted in 10 mL dichloroethane (DCE) using 0.15 mL (0.9 mmol) HDI and 3 µL (0.005 mmol) dibutyltin dilaurate as catalyst. The reaction mixture was stirred vigorously with a mechanical stirrer (Heidolph, RZR2102, Schwabach, Germany) at 200 rpm for one hour, subsequently poured into a Teflon dish, which was kept at 80 °C for 24 h under a constant nitrogen flow and then four days at 100 mbar. The nanocomposite was purified three times by extraction with chloroform and subsequent drying. The synthesis of neat polymer network N-OPDL was carried out by crosslinking pure ^{3}AOPDL without the addition of OPDL@MNP [23]. The GPC measurement, DSC and tensile tests were performed as stated in reference [26].

Cyclic, thermomechanical tests were conducted with standard samples (ISO 527–2/1BB) cut from films on a tensile tester Z1.0 (Zwick, Ulm, Germany) equipped with a thermo-chamber controlled by a Eurotherm control 2408 unit (Eurotherm Regler, Limburg, Germany). In each experiment the strain rate of 5 mm·min^{-1} and a heating and cooling rate of 2 K·min^{-1} was used. Cyclic thermomechanical tensile tests to investigate the actuation were carried out by deforming the samples to ε_{prog} = 50% at T_{high} = 90 °C and equilibrated for 20 min. The samples were then cooled to T_{low} = 40 °C with 2 K·min^{-1} under strain controlled conditions. After a waiting period of 10 min, the stress was unloaded to a value of σ = 50 mN. The samples were heated to T_{sep} with a heating rate of 2 K·min^{-1} under σ = 50 mN, at which the sample contracted to shape A (ε_A). In the reversibility module, the samples were cooled to T_{low}, and after a waiting period of 10 min, reheated to T_{sep}. During cooling the samples elongated to a new shape B (ε_B). The reversibility module was repeated three times with a heating and cooling rate of 2 K·min^{-1}. The actuating temperatures associated to cooling $T_{act,c}$ and melting $T_{act,m}$ were determined at the inflection point of the actuation curve at the maximum of the absolute value of $\Delta\varepsilon/\Delta T$ during elongation and contraction. The fixation efficiency Q_{ef} and reversible elongation ε_{rev} were determined according to the equations 1 and 2, respectively [27].

$$Q_{ef} = \frac{\varepsilon_A(N)}{\varepsilon_{prog}} \, x \, 100\% \qquad (1)$$

$$\varepsilon_{rev} = \frac{l_B(N) - l_A(N)}{l_B(N)} \, x \, 100\% \qquad (2)$$

Where: l_A – sample's length in the shape A, l_B – sample's length in the shape B.

The cyclic, thermomechanical experiments for monitoring the contractual stress (σ_{contr}) during actuation cycles, were carried out by deforming the samples to ε_{prog} = 50 % at T_{high} = 90 °C and equilibrated for 20 min. The samples were then cooled to T_{low} = 40 °C with 2 K·min^{-1} under strain controlled conditions. After 10 min waiting period the sample was unloaded to a stress value of σ = 50 mN. When heated to T_{sep} with a heating rate of 2 K·min^{-1} under σ = 50 mN, the sample contracted to shape A (ε_A). Shape B (ε_B) was obtained by cooling the sample to T_{low} during a waiting period of 10 min. Here, the strain was kept constant and heating to T_{sep} (5 min) was carried out, during which σ_{contr} was recorded. The sample was again cooled to T_{low} followed by a waiting period of 5 min. The heating and cooling cycles were repeated three times.

Results and discussion

The H-NCs showed a homogeneous distribution of covalently integrated MNP in the polymer matrix without any particle sedimentation [26]. When the MNP content was increased, the melting range of the OPDL crystals ($\Delta T_{m,OPDL}$) and the crystallization range ($\Delta T_{c,OPDL}$) were shifted to higher temperature. $\Delta T_{m,OPDL}$ was shifted from 36°C - 76 °C for the homopolymer network (N-OPDL) to 38°C - 80 °C for H-NC5 and to 41°C – 81 °C for H-NC9. On the other hand side, $\Delta T_{c,OPDL}$ was shifted from 20 °C - 57 °C for N-OPDL to

25 °C - 62 °C for H-NC5 and to 37 °C - 65 °C for H-NC9. The melting peak maxima T_m were increased from 73 °C for N-OPDL to 77 °C for H-NC9 (Figure 1). Similarly, T_c was increased from 50 °C for N-OPDL to 61 °C for H-NC9. However, significantly lower values of the T_m and T_c of the H-NC as compared to the precursors ($T_{m,\ ^3AOPDL}$ = 87 °C, $T_{m,\ OPDL@MNP}$ = 87 °C) were attributed to the network formation, which reduced the flexibility of the polymer chains and in this way their crystallization tendency [26]. The $\Delta T_{m,OPDL}$ and $\Delta T_{c,OPDL}$ for N-OPDL and H-NC were higher as compared to the precursors, which enabled sharp transitions with $\Delta T_{m,\ OPDL}$ from 71 °C - 91 °C and $\Delta T_{c,OPDL}$ from 63 °C - 79 °C. These sharp transitions could be attributed to larger and uniform crystal sizes in precursors compared to H-NC. Furthermore, a slight increase in the degree of crystallinity *(DOC)* in H-NC5 (*DOC* = 31%) compared to N-OPDL (*DOC* = 28%) was observed and can be attributed to the MNP acting as nucleating agents for crystallization. However, for H-NC9 with higher MNP content, the *DOC* was decreased to 26%. This decrease of *DOC* could be attributed to a higher crosslinking density which disturbed the crystallization of the nanocomposite [26].

The effect of MNP on elastic properties was investigated by uniaxial tensile testing at 90 °C which is above the $\Delta T_{m,OPDL}$ for all samples. An increasing trend in the elastic modulus *E* by increasing OPDL@MNP content in H-NC was observed (Table 1). The value of *E* was increased from 2.8 MPa for N-OPDL to 3.6 MPa for H-NC9 and can be attributed to the increase in crosslink density (υ_c) [26].

Table 1: Crosslinking density and mechanical properties of the H-NCs and N-OPDL

Sample ID*	υ_c (mol·cm^{-3})[a]	M_c (g·mol^{-1})[b]	$E_{90°C}$ (MPa)[c]	E_{Tsep} (MPa)[d]	ε_b (%)[e]
N-OPDL	4.3×10^{-4}	3710 ± 80	2.8 ± 0.2	1.7 ± 0.3	300 ± 11
H-NC5	4.5×10^{-4}	3650 ± 70	3.5 ± 0.2	2.9 ± 0.2	155 ± 10
H-NC9	4.8×10^{-4}	3620 ± 70	3.6 ± 0.2	4.7 ± 0.2	105 ± 5

*N-OPDL is the neat polymer network, H-NC(x) stands for hybrid nanocomposites, here x is the weight% of the MNP content determined by thermogravimetry. [a]crosslinking density [b]molecular weight between two crosslinks determined by Mooney-Rivlin equation, [c]Elastic modulus at T_{high} = 90±1 °C [d]Elastic modulus and [e]elongation at break determined at T_{sep} enabling maximum actuation capability (T_{sep} = 70±1 °C for N-OPDL, T_{sep} = 71±1 °C for H-NC5, T_{sep} = 75±1 °C for H-NC9)

By applying the Mooney-Rivlin equation, an increase of υ_c from 4.3×10^{-4} mol·cm^{-3} for N-OPDL to 4.8×10^{-4} mol·cm^{-3} for H-NC9 was quantified. At 90 °C, elongation at break (ε_b) values were in the range between 60% and 80%. Also at 90 °C, a slight increase in maximum stress (σ_{max}) was observed when the MNP content was increased. The mechanical analysis particularly at 90 °C indicated that OPDL@MNP provides chemical crosslinks and acts as reinforcing filler with homogenous distribution of MNP [26].

The actuation of the H-NCs and N-OPDL was investigated by cyclic, thermomechanical experiments. All the samples provided an elongation at break $\varepsilon_b > 50\%$ at T_{high} = 90 °C, which is above the melting range of all samples. The test consisted of an initial programming step with a deformation to ε_{prog} = 50 % at T_{high}, followed by three reversible cycles. The values of ε_{prog}, T_{high} and T_{low} were kept constant for all samples, while T_{sep} was varied within the melting range $\Delta T_{m,OPDL}$ of the samples. During initial programming at T_{high} (Figure 1a), the polymer chains were oriented.

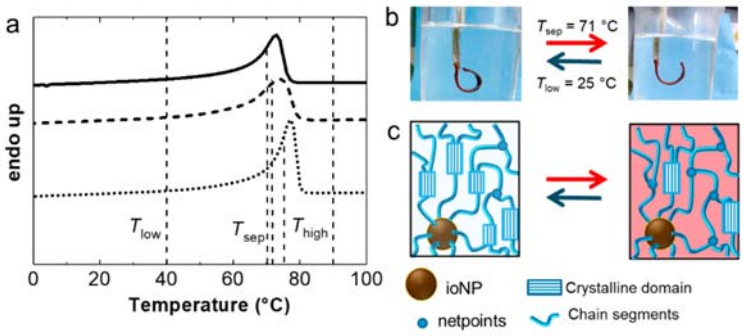

Figure 1 Thermal transitions and mechanism of H-NC actuators: a) DSC thermogram of H-NC indicating the selected values of T_{low}, T_{sep}, T_{high}, N-OPDL (solid line), H-NC5 (dashed line), H-NC9 (dotted line). b) actuation of H-NC5 by heating and cooling. c) Symbolic representation of the molecular mechanism of actuation of the composite.

Cooling the samples to ambient temperature (T_{low} = 25 °C) resulted in the crystallization of the oriented chains and formation of the skeleton. The reversible effect was studied by heating the nanocomposites to T_{sep} to partially melt the crystalline OPDL domains. Heating to T_{sep} caused the partial recovery under stress free conditions and shape A (ε_A) was obtained. Subsequent cooling to T_{low} resulted in directed crystallization of the oriented actuating domains and shape B (ε_B) was obtained. Reheating to T_{high}, melted the actuating domains and the sample shifted to the sample reversibly to shape A because of the melting-induced contraction (MIC) (Figure 1b). The molecular mechanism of the thermal actuation of H-NCs is shown in Figure 1c.

In the first experiment, the actuation capability of the H-NC5 with 5 wt% of MNP content was explored. To optimize the actuation capability, T_{sep} was varied between 69 °C to 72 °C and the values of ε_{rev} and Q_{ef} were determined as function of T_{sep} (Figure 2b). Q_{ef} decreased from 82 ± 3% at T_{sep} = 69 °C to 10 ± 2% at T_{sep} = 72 °C. ε_{rev} increased from 2 ± 0.1% to 8 ± 0.2% when T_{sep} was raised from 69 °C to 71 °C. Referring to the working principle of the actuation under stress free conditions, an increased quantity of AD between T_{low} and T_{sep} of the composite resulted in an increase of ε_{rev}. However, by further increasing T_{sep} = 72 °C, the value of ε_{rev} was decreased to 4 ± 0.3%. When the the sample was heated to T_{sep} = 72 °C (which is near $T_{m,max}$), most of the crystals of the actuating domains were molten and the fraction GD decreased resulting in a lower stabilization of the AD and by this in a lower orientation of the AD and lower value of ε_{rev} [15].

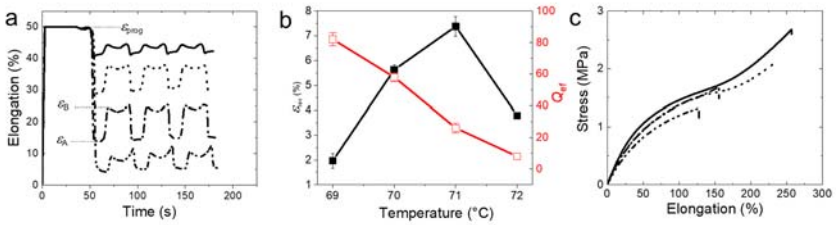

Figure 2 Actuation capability and elastic properties of H-NCs: a) Actuation cycles for H-NC5 at different T_{sep} (solid line 69 °C, dotted line 70 °C, dash dotted line 71 °C and dash dot dotted line 72 °C), b) Actuation parameters of the H-NC5 at different values of T_{sep}. c) Stress-strain behavior of H-NC5 at different T_{sep} (solid line 69 °C, dotted line 70 °C, dash dotted line 71 °C and dash dot dotted line 72 °C)

Table 2: Values of fixation efficiency (Q_{ef}), reversible elongation (ε_{rev}) and contractual stress (σ_{cont}) of H-NCs and N-OPDL

Sample ID	Q_{ef} (%)	ε_{rev} (%)	σ_{cont} (MPa)
N-OPDL	70 ± 1	11.1 ± 0.3	0.30 ± 0.11
H-NC5	44 ± 1	8.2 ± 0.2	0.26 ± 0.01
H-NC9	35 ± 1	3.1 ± 0.3	0.20 ± 0.03

In addition, actuation temperature during cooling $T_{act,c}$, was increased from 63.2 ± 0.2 °C at T_{sep} = 69 °C to 70.1 ± 0.2 °C at T_{sep} = 72 °C. A similar increase in $T_{act,m}$ during heating, from 67.8 ± 0.2 °C at T_{sep} = 69 °C to 73.1 ± 0.4 °C at T_{sep} = 72 °C was observed.

Furthermore, the elastic properties of the H-NC5 at different values of T_{sep} ranging from 69 °C to 72 °C were investigated. The resulting stress-strain graph is shown in Fig. 2c. By increasing T_{sep}, a decrease in E from 2.9 ± 0.2 MPa at 69 °C to 2.49 ± 0.2 MPa at 72 °C was observed, attributed to the decrease of the crystalline OPDL phase. A similar trend in the values of ε_b was also observed. The ε_b was decreased from 255 ± 5% at 69 °C to 125 ± 8% at 72 °C.

To see the actuation capability of H-NC9 with higher MNP content, the sample was programmed at T_{high} = 90 °C and the actuation capability was examined by using different T_{sep} in the melting range 74-77 °C of the OPDL crystalline domain. The sample showed the maximum value of ε_{rev} = 3.1 ± 0.3% at T_{sep} = 75 °C and the Q_{ef} = 35% (Figure 3a). The tensile testing of H-NC9 at optimized T_{sep} = 75 °C, resulted in an $E_{T_{sep}}$ = 4.7 MPa and ε_b of 105 ± 5% (Table 1). Here, a higher value of E for H-NC9 compared to H-NC5 was observed, but a significant decrease in the actuation capability compared to the H-NC5 (5 wt% MNP) was evident. The lower value of ε_{rev} when the MNP content was increased can be attributed to the MNP crosslinks, which impose a constraint against the deformation of the nanocomposite, resulting in a decrease of aligned polymer chain segments contributing to the actuation domains during actuation cycles [18]. However, no significant change in the value of ε_{rev} by increasing number of cycles was observed for both composites.

Furthermore, the actuation capability of the reference network N-OPDL at varied T_{sep} in the melting range from 68 °C to 71°C was investigated. An optimized actuation of ε_{rev} = 11% was observed at T_{sep} = 70 °C (Table 2, Fig. 3a), which was 38% higher compared to H-NC5 and 220% higher compared to H-NC9. This significant increase of actuation capability of N-OPDL could be attributed to the higher orientation of the actuating domain resulting an increased crystal-induced elongation (CIE) compared to the nanocomposites. Nevertheless, a lower $E_{T_{sep}}$ of 1.7 ± 0.3 MPa and a higher ε_b of 300 ± 20% at T_{sep} = 70 °C compared to H-NC were observed (Table 1).

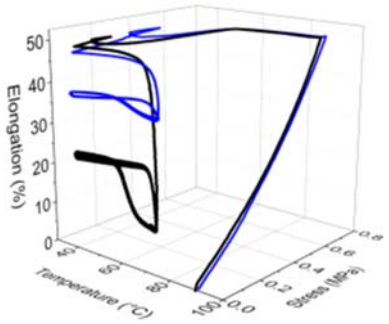

Figure 3 Cyclic thermo-mechanical tensile tests: for H-NC9 at T_{sep} = 75 °C (blue) and pure network N-OPDL at T_{sep} = 70 °C (black)

To see the effect of MNP on σ_{contr} of the actuators, thermo-mechanical experiments by application of a constant ε_{prog} and an optimized T_{sep} were carried out. During cyclic heating and cooling of the programmed samples under constant strain conditions, a lowering of σ_{contr}, when the MNP content was increased could be observed. When the samples were heated to T_{sep}, σ_{contr} was increased and reached a maximum value, whereas during cooling, σ_{contr} was decreased again to the original level owing to the formation of crystallites. For the N-OPDL without MNP addition, a maximum value of $\sigma_{contr} = 0.3 \pm 0.1$ MPa was observed. For the nanocomposite sample H-NC5, the σ_{contr} was decreased to 0.26 ± 0.02 MPa, while for H-NC9, a minimum value of $\sigma_{contr} = 0.2 \pm 0.03$ MPa was observed (Table 1). The lowering of the σ_{contr} could be attributed to the increasing MNP content, which hindered the crystallization and decreased the elasticity of the H-NC. Nevertheless, a slight lowering of σ_{cont} for H-NC9 by increasing the number of heating/cooling cycles was observed. The σ_{contr} of the N-OPDL and the H-NCs are shown in Figure 4.

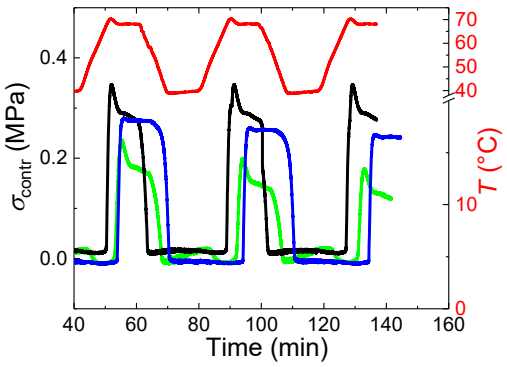

Figure 4 Stress generation during actuation experiments by cyclic heating and cooling: exemplarily provided for N-OPDL with an optimized $T_{sep} = 70$ °C and $T_{low} = 40$ °C, black line (N-OPDL), blue line (H-NC5) and green line (H-NC9).

Summary

Synthesis of hybrid SMPA by covalent integration of MNP was carried out and the actuation performance, contractual stress (σ_{contr}) and the relevant material properties were compared to the PPDL-based homopolymer network. By increasing the MNP content in H-NC, an increase in the crosslinking density was observed, while the degree of crystallinity was decreased. The melting and crystallization range of the OPDL crystals were shifted to higher temperatures by increasing MNP content. At T_{high} and at T_{sep} an increase in the elastic moduli was observed when the MNP content was increased, while the value of elongation at break ε_b was decreased. The extent of actuation could be controlled by changing T_{sep} or MNP content in these H-NC. The increase in the actuation performance by increasing T_{sep} was attributed to the increasing volume fraction of the actuating domain. However, the actuation performance was lowered by increasing MNP content and was attributed to the restraining effect of the MNP on the reversible movements. Furthermore, application of a constant strain to the programmed samples enabled the determination of σ_{contr} during actuation experiments. Here, again a decrease in σ_{contr} by increasing MNP content was observed.

In conclusion, a synergism between the nanoparticles and the polymer could be exploited to enhance the Young's moduli of the actuating nanocomposite but for the sake

of a simultaneous reduction in the actuation capability. Nevertheless, the demonstrated feasibility of covalent integration of MNP in H-NCs might stimulate future work in the development of soft actuators by using other types of nanoparticles like anisotropic nanoparticles to provide a directed reinforcement and by this a directed enhancement of the actuation performance.

Acknowledgement

This work was supported by the Helmholtz-Association through programme-oriented funding.

References

1. P. Lochmatter, G. Kovacs and P. Ermanni, *Smart Materials & Structures* **16** (4), 1415-1422 (2007).
2. J. Shintake, S. Rosset, B. Schubert, D. Floreano and H. Shea, *Adv Mater* **28** (2), 231-238 (2016).
3. W. Wang, X. Z. Wang, F. T. Cheng, Y. L. Yu and Y. T. Zhu, *Prog Chem* **23** (6), 1165-1173 (2011).
4. Q. Zhao, X. X. Yang, C. X. Ma, D. Chen, H. Bai, T. F. Li, W. Yang and T. Xie, *Materials Horizons* **3** (5), 422-428 (2016).
5. L. Gao, G. Q. Guo, M. J. Liu, Z. G. Tang, L. X. Xie and Y. P. Huo, *Rsc Adv* **7** (63), 40005-40014 (2017).
6. X. Li, X. B. Cai, Y. F. Gao and M. J. Serpe, *J Mater Chem B* **5** (15), 2804-2812 (2017).
7. J. R. Wang, J. F. Wang, Z. Chen, S. L. Fang, Y. Zhu, R. H. Baughman and L. Jiang, *Chem Mater* **29** (22), 9793-9801 (2017).
8. H. R. Jiang, C. S. Li and X. Z. Huang, *Nanoscale* **5** (12), 5225-5240 (2013).
9. C. Ohm, M. Brehmer and R. Zentel, *Adv Mater* **22** (31), 3366-3387 (2010).
10. Y. L. Yu, *Abstr Pap Am Chem S* **245** (2013).
11. K. Uh, B. Yoon, C. W. Lee and J. M. Kim, *ACS Appl Mater Inter* **8** (2), 1289-1296 (2016).
12. X. L. Wang, I. K. Oh and T. H. Cheng, *Polym Int* **59** (3), 305-312 (2010).
13. N. Festin, C. Plesse, P. Pirim, C. Chevrot and F. Vidal, *Sensor Actuat B-Chem* **193**, 82-88 (2014).
14. E. H. Lee, H. M. Kim, S. K. Lim, K. S. Kim and I. J. Chin, *Mol Cryst Liq Cryst* **492**, 11-19 (2008).
15. M. Behl, K. Kratz, U. Noechel, T. Sauter and A. Lendlein, *P Natl Acad Sci USA* **110** (31), 12555-12559 (2013).
16. A. Biswas, V. K. Aswal, P. U. Sastry, D. Rana and P. Maiti, *Macromolecules* **49** (13), 4889-4897 (2016).
17. M. Farhan, T. Rudolph, U. Nochel, W. Yan, K. Kratz and A. Lendlein, *ACS Appl Mater Inter* **9** (39), 33559-33564 (2017).
18. F. J. Ge, X. L. Lu, J. Xiang, X. Tong and Y. Zhao, *Angew Chem Int Edit* **56** (22), 6126-6130 (2017).
19. R. Fuhrer, E. K. Athanassiou, N. A. Luechinger and W. J. Stark, *Small* **5** (3), 383-388 (2009).
20. J. Sommertune, A. Sugunan, A. Ahniyaz, R. Bejhed, A. Sarwe, C. Johansson, C. Balceris, F. Ludwig, O. Posth and A. Fornara, *International Journal of Molecular Sciences* **16** (8), 19752 (2015).
21. M. Y. Razzaq, M. Behl and A. Lendlein, *Nanoscale* **4** (20), 6181-6195 (2012).
22. J. Thevenot, H. Oliveira, O. Sandre and S. Lecommandoux, *Chem Soc Rev* **42** (17), 7099-7116 (2013).
23. M. Y. Razzaq, M. Behl, K. Kratz and A. Lendlein, *Adv Mater* **25** (40), 5730-+ (2013).
24. L. Wang, M. Y. Razzaq, T. Rudolph, M. Heuchel, U. Nöchel, U. Mansfeld, Y. Jiang, O. E. C. Gould, M. Behl, K. Kratz and A. Lendlein, *Materials Horizons* **5**, 861-867 (2018).
25. M. Y. Razzaq, M. Behl, U. Frank, J. Koetz, W. Szczerba and A. Lendlein, *J Mater Chem* **22** (18), 9237-9243 (2012).
26. M. Y. Razzaq, M. Behl, U. Nochel and A. Lendlein, *Polymer* **55** (23), 5953-5960 (2014).
27. M. Behl, K. Kratz, J. Zotzmann, U. Nochel and A. Lendlein, *Adv Mater* **25** (32), 4466-4469 (2013).